



The role of polymer molecular weight distribution in drag-reducing turbulent flows

F. Serafini¹ , F. Battista¹ , P. Gualtieri¹ and C.M. Casciola¹ 

¹Department of Mechanical and Aerospace Engineering, Sapienza University of Rome via Eudossiana 18, Rome 00184, Italy

Corresponding author: F. Serafini, francesco.serafini@uniroma1.it

(Received 26 July 2024; revised 8 October 2024; accepted 14 November 2024)

Drag reduction induced by a polydisperse solution of polyethylene oxide is investigated by direct numerical simulations of the Navier–Stokes equations coupled with the Lagrangian evolution of the polymers, modelled as dumbbells. Simulation parameters are chosen to match the experimental conditions of Berman (1977), who measured the polymer molecular weight distribution. Drag reduction is induced only by the few high molecular weight polymers fully stretched by the turbulent flow, whilst the hundreds of parts per million of low molecular weight chains are ineffective.

Key words: polymers, pipe flow, turbulence simulation

1. Introduction

In wall-bounded flows, the laminar–turbulent transition is responsible for a sharp increase in drag. Therefore, a large interest has been devoted to techniques able to reduce friction (Du & Karniadakis 2000). Among many possibilities, the addition of a few parts per million in weight (wppm) of long linear polymers in a Newtonian solvent is known to produce up to 80 % drag reduction (Procaccia *et al.* 2008). This phenomenon is due to the mechanical interaction between polymers and turbulence (Xi 2019) and has been known since the experimental studies of Toms (1949).

Experimental results (Virk (1975); McComb & Rabie (1982) to cite a few) have been the main source of information for years but they did not provide in-depth details on the polymerturbulence interaction and opened the way for different interpretations, the most famous ones ascribed to Lumley (1969) and De Gennes (1986). The crucial point observed by Lumley (1973) is that the polymers interact with the turbulent field when their relaxation time τ is of the order of the turbulent smallest time scale $\tau_* = \nu/u_\tau^2$, where

ν is the kinematic viscosity and u_τ is the friction velocity. When the ratio between the two quantities, named the Weissenberg number $Wi_\tau = \tau/\tau_*$, exceeds order 1, polymers undergo the coilstretch transition. Lumley's theory predicts that the polymer molecules expand under the turbulent fluctuating strain rate and their effect is to damp the small eddies.

Experiments with DNA chains show that a concentration of 1 wppm is sufficient to achieve a consistent drag reduction and Choi *et al.* (2002) showed that the turbulent flow largely stretches the DNA chains. By direct numerical simulations of DNA dilute polymer solutions, Serafini *et al.* (2022) showed that polymer stretching is essential for drag reduction. In particular, only the fully stretched polymers are effective, whilst unstretched polymers do not produce any effect.

Despite the previous examples agreeing with Lumley's idea, there are many other experiments where polymer stretching does not seem essential for drag reduction. With synthetic polymers (e.g. polyethylene oxide, PEO), estimations based on average parameters, see Sreenivasan & White (2000), suggest that drag reduction occurs even when polymers are poorly stretched. Differently from experiments with DNA, experiments involving synthetic polymers are generally characterised by a small value of the Weissenberg number (even less than unity, Virk (1975)), and are thus expected to be mildly stretched. However, drag reduction can still be achieved, but larger polymer concentrations are required, often a hundred times larger than needed with DNA. A qualitative explanation of these experiments where large polymer stretching is not expected to occur can be found in the theory proposed by De Gennes (1986). The first observation at the basis of the elastic theory of Tabor & De Gennes (1986) is that the polymers do not produce measurable changes in viscosity if moderately stretched. Nonetheless, turbulence can be modified if the polymer concentration is large enough that the suspension elastic energy is comparable to the solvent kinetic energy of the smallest eddies.

At the time, no information was available from experiments to deeply understand the role of polymer stretching and concentration in drag reduction. Significant advances have been made thanks to direct numerical simulation (DNS) of polymeric turbulence, mostly based on Eulerian viscoelastic constitutive models (Alves *et al.* 2021), which has been an additional source of information since the late 1990s (Sureshkumar *et al.* 1997; Dimitropoulos *et al.* 1998; De Angelis *et al.* 2002). Simulations provided a qualitative understanding of polymer drag reduction in turbulent flows and different interpretations of the phenomenon have been proposed. Drag reduction has been interpreted either in terms of an effective viscosity induced by the polymers (Benzi *et al.* 2006) or as the result of a transfer of elastic energy, stored by the polymers near the wall and released in the buffer and logarithmic layers (Min *et al.* 2003). Besides the different interpretations, they could not fully clarify the contrasting information found in the experiments, as far as the role played by polymer stretching and concentration is concerned. The statistics provided by those simulations, however, consider polymers that are longer than their maximum length (Vincenzi *et al.* 2015) and the values of concentrations required for drag reduction exceed by far the experimental ones (Sureshkumar *et al.* 1997).

The contrasting conclusions presented above led us to suspect that different drag reduction mechanisms may be at work, with drag reduction obtainable in two different ways depending on the nature of the specific polymers involved. Interestingly, in his review Lumley (1969) recognised the use of polydisperse polymers as a possible misleading factor for the characterisation of the onset of drag reduction, as the highest molecular weight chains may have a 'disproportionate' effect. A crucial difference between DNA and PEO solutions is that the former are monodisperse while the latter typically have a broad distribution of molecular weights (Bird *et al.* 1987). The experiments of Berman (1977)

confirmed Lumley's doubt, showing that drag reduction is strongly conditioned by polydispersity, with the onset mainly caused by the highest molecular weight polymers of the distribution. Indeed, the polymer relaxation time approximately grows with the square of the molecular weight, see Doi *et al.* (1988). The reason for this behaviour was not completely clarified and this uncertainty persisted over the years. Recent experimental investigations by Brandfellner *et al.* (2024) reanalysed the role of the molecular weight distribution, employing multiple linear regression to find the link between weight fractions of polyacrylamide and drag reduction. However, according to the authors, the fitting lacks physical meaning since some coefficients are negative, confirming that the relation between polydispersity and drag reduction requires additional physical information to be fully understood.

To investigate drag reduction by a polydisperse solution we exploit a recently developed hybrid EulerianLagrangian methodology (described in § 2) for simulations of polymer solutions, able to reproduce polymer chains with realistic parameters (Serafini *et al.* 2023) and provide reliable polymer stretching statistics. The analysis, presented in § 3, aims to explain the role of different molecular weight fractions in polymer drag reduction and to provide a unique explanation for the conflicting behaviours of the polymers observed in experiments and simulations.

2. Methodology

The dynamics of the polymer solution is simulated by evolving the Navier–Stokes equation for the motion of the solvent

$$\nabla \cdot \mathbf{u} = 0, \quad \frac{\partial \mathbf{u}}{\partial t} + \nabla \cdot (\mathbf{u} \otimes \mathbf{u}) = -\nabla p + \frac{1}{Re} \nabla^2 \mathbf{u} + \mathbf{F}, \quad (2.1)$$

alongside the Lagrangian evolution of the polymers. Polymers and fluid exchange friction forces that are proportional to the relative velocity between polymer beads and solvent. The dynamics is simulated in a pipe, thus the system (2.1) is solved in cylindrical coordinates (θ, r, z) and completed with the no-slip condition, $\mathbf{u}(t, \theta, r = 1, z) = 0$ at the wall. The system is reported in dimensionless form, obtained using as reference quantities the pipe radius ℓ_0^* , the solvent density ρ^* , the solvent viscosity μ^* and the bulk velocity $U_{b,n}^* = Q^*/(\pi \ell_0^{*2})$, given the volumetric flow rate Q^* of the Newtonian case (without added polymers). An asterisk is used as a superscript to denote dimensional quantities. In (2.1), \mathbf{u} is the solvent velocity, p the hydrodynamic pressure, \mathbf{F} the force field that the polymers exert on the solvent. The dimensionless parameter $Re = \rho^* U_{b,n}^* \ell_0^*/\mu^*$ is the Reynolds number. The motion of the polymer solution is sustained by imposing a constant pressure gradient. This allows us to fix the average shear stress at the wall $\tau_w^* = \mu^* \partial \langle u_z^* \rangle / \partial r^*$ (u_z is the axial component of the velocity field). In dimensionless terms, this corresponds to fixing the friction Reynolds number $Re_\tau = \rho^* u_\tau^* \ell_0^*/\mu^*$, where $u_\tau^* = \sqrt{\tau_w^*/\rho^*}$ is the friction velocity.

Since the average wall shear stress is fixed, the effect induced by the polymers is measured in terms of an increase in the bulk velocity and can be evaluated through the variation of the friction factor $f = 8\tau_w^*/(\rho^* U_b^{*2})$. The drag reduction is measured via the parameter

$$DR = \frac{f^{(0)} - f^{(p)}}{f^{(0)}} = 1 - \left(\frac{U_{b,n}}{U_{b,p}} \right)^2, \quad (2.2)$$

with n and p denoting the Newtonian and the polymeric cases, respectively.

The polymer chains are modelled as dumbbells, namely two beads at position $\mathbf{x}_{1/2}$ connected by a nonlinear entropic spring. The beads exchange the friction forces

$$\mathbf{D}_{1/2} = \gamma \left(\check{\mathbf{u}}_{1/2} - \frac{d\mathbf{x}_{1/2}}{dt} \right), \quad (2.3)$$

with the solvent, given the beads' friction coefficient γ and the undisturbed velocity of the solvent $\check{\mathbf{u}}_{1/2}$ at the position $\mathbf{x}_{1/2}$ (Maxey & Riley (1983)). Since the mass of the beads can be safely neglected, Newton's law for each bead reduces to the instantaneous balance between friction forces and the entropic elastic and Brownian forces that tend to restore the equilibrium configuration in a quiet solvent, see Bird *et al.* (1987),

$$0 = \gamma \left(\check{\mathbf{u}}_{1/2} - \frac{d\mathbf{x}_{1/2}}{dt} \right) \pm k \frac{\mathbf{r}}{1 - \|\mathbf{r}\|^2/L^2} + r_{eq} \sqrt{\frac{2k\gamma}{3}} \xi_{1,2}, \quad (2.4)$$

where $\mathbf{r} = \mathbf{x}_2 - \mathbf{x}_1$ is the polymer end-to-end vector, r_{eq} is the polymer equilibrium size in a quiet solvent set by the white noise $\xi_{1/2}$, $k = 3k_B T / r_{eq}^2$ is the entropic spring stiffness (k_B is the Boltzmann constant and T the absolute temperature) and L the polymer contour length.

For a population of N polymers, the evolution of the j th dumbbell can be conveniently rewritten in terms of the polymer centre $\mathbf{x}_c^{(j)} = (\mathbf{x}_1^{(j)} + \mathbf{x}_2^{(j)})/2$ and normalised end-to-end vector $\mathbf{h}^{(j)} = \mathbf{r}^{(j)}/L$

$$\begin{cases} \frac{d\mathbf{x}_c^{(j)}}{dt} = \frac{\check{\mathbf{u}}_1^{(j)} + \check{\mathbf{u}}_2^{(j)}}{2} + \frac{r_{eq}}{\sqrt{3} \text{Wi}} \frac{\xi_1^{(j)} + \xi_2^{(j)}}{2} \\ \frac{d\mathbf{h}^{(j)}}{dt} = \frac{\check{\mathbf{u}}_2^{(j)} - \check{\mathbf{u}}_1^{(j)}}{L} - \frac{\mathbf{h}^{(j)}}{\text{Wi}(1 - \|\mathbf{h}^{(j)}\|^2)} + \frac{r_{eq}}{L\sqrt{3} \text{Wi}} (\xi_2^{(j)} - \xi_1^{(j)}) \end{cases}. \quad (2.5)$$

Despite its simplicity, the finitely extensible nonlinear elastic (FENE) dumbbell model is known to provide an accurate description of the polymer dynamics in wall-bounded turbulence, see Zhou & Akhavan (2003) and Serafini *et al.* (2024). In (2.5), $\text{Wi} = \tau^*/(\ell_0^*/U_{b,n}^*)$ is the Weissenberg number. It can be proved that, for dumbbells, $\text{Wi} = \gamma/(2k)$. The beads exchange the friction forces with the fluid, thus the polymer back-reaction field on the solvent is

$$\mathbf{F} = - \sum_{j=1}^N \mathbf{D}_1^{(j)} \delta(\mathbf{x} - \mathbf{x}_1^{(j)}) + \mathbf{D}_2^{(j)} \delta(\mathbf{x} - \mathbf{x}_2^{(j)}), \quad (2.6)$$

where δ is the Dirac delta function centred at $\mathbf{x}_{1/2}$.

Equations (2.1) and (2.5), with the polymer forcing (2.6), are numerically solved (DNS) on a staggered grid using a projection method to enforce velocity solenoidality. In the axial direction, the periodic boundary condition is imposed. Time integration is performed using a four-step, third-order, Runge–Kutta low-storage scheme, while second-order finite differences are employed for the spatial discretisation. The domain dimensionless size is $(2\pi \times 1 \times 6\pi)$ and the grid points are $[N_\theta \times N_r \times N_z] = [1408 \times 239 \times 4224]$. The grid is non-homogeneous in the radial direction to ensure a higher resolution close to the wall and is set to resolve the most demanding case, i.e. $Re_\tau = 320$, with a maximum grid spacing of 1.4 wallunits. Statistics are collected once the flow rate has reached the statistical steady state and averages have been performed on 200 uncorrelated fields. The singular polymer forcing (2.6) is regularised according to the exact regularised point particle method, see Gualtieri *et al.* (2015). The method exploits the solution of the

unsteady Stokes equation to diffuse the reaction field on the computational grid (Gualtieri *et al.* 2015; Battista *et al.* 2019). The Dirac delta function at time $t - \epsilon_R$ is regularised at time t , thus the non-singular forcing

$$F = \sum_{j=1}^N -\frac{\mathbf{D}_1^{(j)}(t-\epsilon_R)}{(4\pi\nu\epsilon_R)^{3/2}} e^{-\frac{\|\mathbf{x} - \mathbf{x}_1^{(j)}(t-\epsilon_R)\|^2}{4\nu\epsilon_R}} - \frac{\mathbf{D}_2^{(j)}(t-\epsilon_R)}{(4\pi\nu\epsilon_R)^{3/2}} e^{-\frac{\|\mathbf{x} - \mathbf{x}_2^{(j)}(t-\epsilon_R)\|^2}{4\nu\epsilon_R}}, \quad (2.7)$$

can be represented on the discrete grid. The boundary condition on the solid wall is accounted for by using the method of images, see Battista *et al.* (2019) for a complete account of the approach.

Simulation parameters are chosen to match the one used by Berman (1977) in his experimental campaign. Concerning the fluid, the parameters to be matched are the kind of solvent (water in this case) with its density ρ^* and dynamic viscosity μ^* , the pipe radius ($\ell_0^* = 2.77$ mm in the experiment) and the friction Reynolds number Re_τ (and the corresponding bulk Reynolds number Re of the Newtonian case). To solve the NavierStokes equation, only the Reynolds number is needed, while the other mentioned dimensional parameters are required to derive the polymer dimensionless quantities. Berman (1977) analysed the drag reduction of a dilute aqueous solution (400 wppm) of PEO (Polyox N-80) for friction Reynolds numbers in the range 150 – 800 and estimated the molecular weight distribution by gel chromatography. The procedure he used could not characterise the molecular weight below 2.5×10^5 , thus only the tail of the molecular weight distribution is available. Nevertheless, the experimental data show that only this tail is relevant for drag reduction, at least at the moderate Reynolds numbers at which the onset occurs. The measured tail ($M^* > 2.5 \times 10^5$) amounts to a concentration of 17.5 wppm compared with an overall concentration of 400 wppm. To reproduce the molecular weight distribution we selected ten different values of the contour length and computed the polymer concentration needed to replicate the experimental sample. Finally, we performed DNSs in the numerically achievable range of friction Reynolds number 180 – 320. As reference data for PEO, we use the information from Virk’s experimental review, which reports a contour length of $L_0^* \approx 6 \mu\text{m}$ and a relaxation time of approximately $\tau_0^* = 3 \times 10^{-4}$ s for a PEO sample with average molecular weight $M_0^* \approx 5.7 \times 10^5$ g mol $^{-1}$. Contour length and relaxation time of the polymers with different molecular weights M^* can be estimated according to the Rouse scaling (Doi *et al.* 1988), namely $L^* = L_0^*(M^*/M_0^*)$ and $\tau^* = \tau_0^*(M^*/M_0^*)^2$. In Berman’s paper, the tail of the molecular weight distribution used in the experiment is reported in terms of cumulative mass (in grams) and molecular weight. For convenience, we report the experimental distribution in figure 1(a) using the cumulative concentration in wppm. The blue dots denote the concentration of the selected ten polymer populations.

The friction coefficient γ^* , although not directly measurable, is related to the polymer relaxation time τ^* and the polymer equilibrium size r_{eq}^* , which can be experimentally measured, see Virk (1975). For a dumbbell, $\gamma^* = 6\tau^*k_B^*T^*/r_{eq}^{*2}$. However, the bead friction coefficient is not the relevant quantity that characterises the dynamics of the polymer solution. The polymer effect on the solvent depends on the quantity $\mu_p^* = c_o^*\gamma^*L^{*2}$, rather than the concentration or the bead friction coefficient alone (Serafini *et al.* 2023). For convenience, we recall that the feedback-forcing field, which can be written in terms of the end-to-end vector using (2.4), can be recast as the divergence of an extra-stress

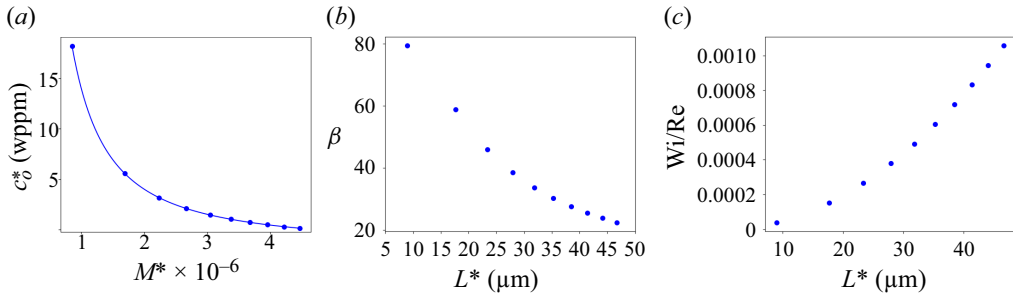


Figure 1. Panel (a) shows the tail of the molecular weight distribution in terms of cumulative concentration (wppm). Panel (b) shows the ratio between the polymer and solvent viscosities for the different polymer populations. Panel (c) shows the ratio of the Weissenberg number and the Reynolds number for the different polymer populations.

tensor, $\mathbf{F} = \nabla \cdot \mathbf{T}_p$, whose leading order reads

$$\mathbf{T}_p \simeq \frac{\beta}{2 \text{Wi} \text{Re}} \sum_{j=1}^N \frac{\mathbf{h}^{(j)} \otimes \mathbf{h}^{(j)}}{1 - \|\mathbf{h}^{(j)}\|^2} \frac{\delta(\mathbf{x} - \mathbf{x}_c^{(j)})}{c_o}, \quad (2.8)$$

where $\beta = \mu_p^*/\mu^*$. It is proved in Serafini *et al.* (2023) that, provided there are a sufficiently high number of polymers, the dynamics of a polymer suspension for given Weissenberg and Reynolds numbers only depends on β and not on the singular parameters c_o^* , γ^* and L^* . The same dynamics can be thus reproduced by a simulation with a lower c_o^* and a larger γ^* , such that β remains constant, to contain the computational cost. This point is crucial since the actual number of polymer chains cannot be computationally afforded. For instance, the population with the smallest molecular weight would require a number of polymers of approximately 10^{13} , an unaffordable number with current (and to come!) computational resources. Here, each population has 10^8 dumbbells, for an overall number of polymers of 10^9 , and the friction coefficient is selected to obtain the desired value of μ_p^* . Figure 1(b) reports the ratio β between polymer viscosity μ_p^* and solvent viscosity μ^* for the ten different polymer populations parametrised in terms of their contour length L^* .

Given the varying molecular weight, the different polymer populations have different Weissenberg numbers. To account for the varying Reynolds number in the simulations, the dependence of the Weissenberg number on the polymer contour length is reported in figure 1(c) in terms of the ratio Wi/Re . This ratio is nothing but the relaxation time τ^* normalised with the viscous time scale ℓ_0^{*2}/ν^* . For each simulation, the Weissenberg number Wi of the polymer populations can be derived by multiplying this quantity by the Reynolds number, while the Weissenberg number in internal units Wi_τ is obtained by multiplication with the square of the friction Reynolds number.

The strong computational demand of the simulations can be nowadays afforded thanks to massive parallelisation on graphics processing units available on modern pre-exascale high performance computing architectures (Leonardo supercomputer facility @ Cineca (Turisini *et al.* 2023)).

3. Results

Figure 2(a) reports the molecular weight distribution used in the simulations. In particular, the black-filled circles denote the concentrations (in wppm) of the selected contour lengths L needed to reproduce the experimental distribution. In the experiment, where different

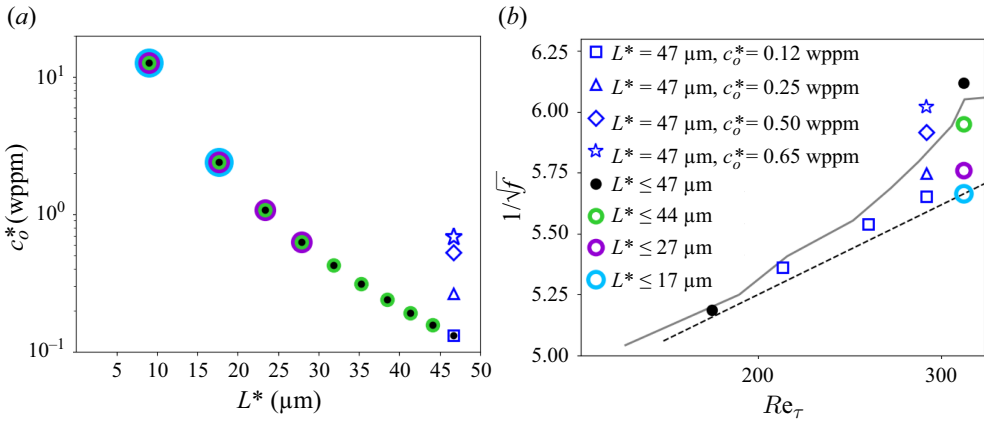


Figure 2. Panel (a) shows the concentration of different contour length polymers to replicate the experimental distribution measured by Berman (1977). Panel (b) shows the inverse of the square root of the friction factor f vs friction Reynolds number Re_τ ; different colours and symbols refer to the different fractions in terms of the polymer population marked by the same colour and symbol in panel (a) (different symbol size is only used for visualisation purposes). The solid grey line is the experimental curve of Berman (1977) and the dashed black line is the Prandtl–Karman Newtonian law.

molecular weight polymers are mixed, the Weissenberg number ranges between 0 and 100, see figure 1(c). Given the huge amount of low molecular weight polymers, the resulting average Weissenberg number is below 1. Thus, a characterisation of the polymer solution with an average Weissenberg number cannot reveal the relation between drag reduction and polymer stretching.

Figure 2(b) reports the friction factor f measured by simulating Berman’s molecular weight distribution. The comparison with the experimental results (black circles vs solid grey line) shows excellent quantitative agreement. Consistently with the experimental data, no drag reduction is measured at $Re_\tau = 180$ and 15% drag reduction is obtained at $Re_\tau = 320$. The green, violet and sky blue rings refer to simulations with only fractions of the polymer population: the green rings refer to the entire population deprived of the subpopulation of the longest polymers, the violet ones account for the first four shortest polymer subpopulations and the sky blue rings involve only the two shortest subpopulations. Drag reduction is largely associated with the longest population alone, while the two shortest subpopulations do not produce any effect. This confirms that the shortest polymers in the experimental distribution can be safely neglected as ineffective. This result is consistent with Lumley’s intuition on the effect of polydispersity, given the ‘disproportionate’ effect of the highest molecular weight sample.

The numerical data allow for quantification of the elongation of the polymer molecules, information not available in the experiments with polydisperse polymers. Figure 3 reports the amount of polymers, in terms of concentration in wppm, with extension $H = \|\mathbf{h}\|$ above H_0 for the ten selected polymer contour lengths (see legend)

$$c_{H \geq H_0}^*(L^*) = c_o^*(L^*) \int_{H_0}^1 p(\sigma) d\sigma, \tag{3.1}$$

where p denotes the probability density function of the end-to-end distance. Panel (a) shows that, at $Re_\tau = 320$, the polymer solution contains highly extended polymers, i.e. characterised by a finite probability of finding polymers with H close to 1. The size of the fully extended population increases with the Reynolds number (see the two panels

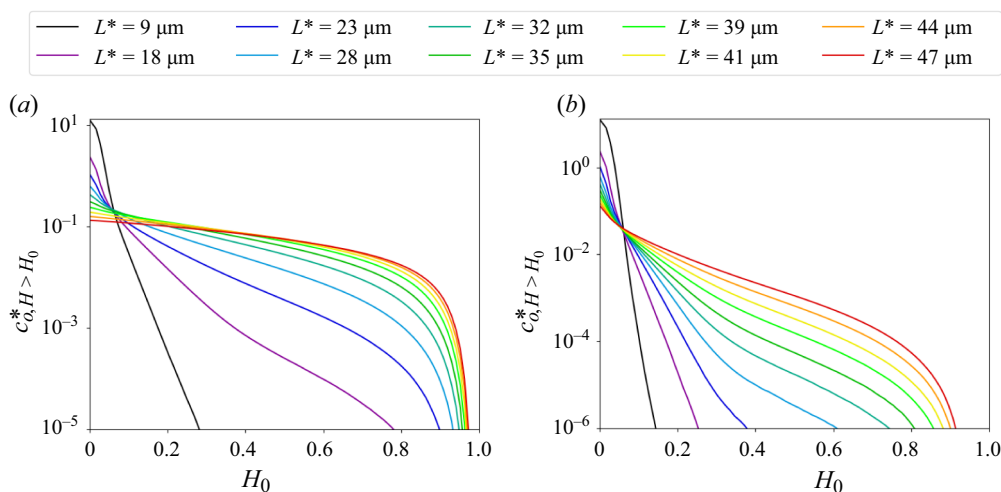


Figure 3. Cumulative distribution of normalised polymer extension H for the selected contour length L at friction Reynolds numbers $Re_\tau = 320$ (a) and $Re_\tau = 180$ (b).

corresponding to $Re_\tau = 320$ and $Re_\tau = 180$) and with the polymer contour (see different colours). Indeed, the Weissenberg number increases with both $Wi_\tau \propto Re_\tau$ and $Wi_\tau \propto L^2$. At $Re_\tau = 180$, shown in panel (b), the number of fully stretched polymers is insignificant and no drag reduction is observed. For instance, the longest population ($L^* = 47 \mu\text{m}$) shows a number of polymers stretched beyond $H_0 = 0.8$ at $Re_\tau = 180$ that is approximately three orders of magnitude smaller than that at $Re_\tau = 320$. At $Re_\tau = 320$ the two shortest populations (black and purple lines in panel a) show a negligible number of fully elongated polymers and do not contribute to drag reduction. Indeed, the polymer population with $L^* < 18 \mu\text{m}$ shows an amount of polymer stretched beyond $H_0 = 0.8$ that is approximately four orders of magnitude smaller than the populations longer than $L^* = 30 \mu\text{m}$.

Drag reduction is due to the highly extended polymers also in the case of polydisperse solutions of synthetic polymers, even if the Weissenberg number is significantly smaller than the case of monodisperse DNA. Indeed, the two shortest subpopulations can be removed with no harm from the suspension, despite exceeding by two orders of magnitude in concentration all of the other subpopulations. Quantitatively, an approximate concentration of 3 wppm of polymers longer than $20 \mu\text{m}$ is responsible for the entire drag reduction at $Re_\tau = 320$, a very small amount if compared with the 400 wppm of the full experimental sample. It is crucial to note that, when the irrelevant low molecular weight polymers are neglected, the concentration of the effective polymers is consistent with the typical concentration used in experiments with monodisperse DNA (few wppm).

The remaining issue concerns the role played by the polymer viscosity μ_p^* in the onset of drag reduction. For this purpose, additional simulations with varying concentration were run, which considered only the longest population, the one with the largest probability of getting stretched. The open squares in figure 2(b) correspond the friction measured by considering 0.12 wppm ($\beta = 22$) of the $47 \mu\text{m}$ long polymers at three different Reynolds numbers, $Re_\tau = 210, 260, 290$. Such a small quantity of polymers is not able to generate any drag reduction. At $Re_\tau = 290$ we also considered three additional solutions with concentration $c_o = 0.25, 0.5, 0.65$ wppm ($\beta = 44, 88, 115$), marked with an open triangle, an open diamond and an open star, respectively. Data show that the increase in concentration provides a remarkable effect on drag reduction (DR), measured at approximately 5%, 10% and 13%, respectively, corresponding to an almost linear increase,

in agreement with Berman’s measurement with fractions of high molecular weight polymers.

In conclusion, very large polymer stretching is the essential ingredient to explain the onset of drag reduction, even in the case of polydisperse solutions for which a characterisation in terms of bulk parameters (concentration and Weissenberg number) would have suggested mild elongation. This brought De Gennes (1986) to propose two different scenarios to explain the modification of turbulence depending on polymer concentration and molecular weight: a first occurring when the polymers are still far from full extension and large concentrations are required, a second occurring when the polymers may be fully elongated. Here, we show that the first scenario is not realised, even for a polymer solution of 400 wppm of PEO with a relatively small average molecular weight, because of polydispersity. Consistently with the experimental observation of Berman, we showed that most of the polymers are ineffective and just a spoonful with high molecular weight induces drag reduction. The highest molecular weight polymers of the distribution exhibit large stretching, eventually realising the second scenario. Consistently with the idea of Lumley (1969), we try to relate the drag reduction to the increase of extensional viscosity. An attempt was also made by Berman (1977) and a correlation between extensional viscosity and drag reduction is reported in the experiments (Escudier *et al.* 1999) and also observed in numerical simulations (Dimitropoulos *et al.* 1998; Serafini *et al.* 2022). Starting from the polymer stress defined in (2.8), the dimensionless increment of extensional viscosity can be derived from its definition

$$\Delta\eta = Re \frac{\mathbf{T}_{p11} - \mathbf{T}_{p33}}{E_{11}} = \sum_{j=1}^N \frac{\beta}{2 Wi} \frac{\|\mathbf{h}^{(j)}\|^2}{1 - \|\mathbf{h}^{(j)}\|^2} \frac{r_1^{(j)2} - r_3^{(j)2}}{E_{11}^{(j)}} \frac{\delta(\mathbf{x} - \mathbf{x}_c^{(j)})}{c_o}, \quad (3.2)$$

where $r_\alpha^{(j)} = (\mathbf{h}^{(j)} \cdot \hat{\mathbf{e}}_\alpha) / \|\mathbf{h}^{(j)}\|$, E_{11} is the largest eigenvalue of $\mathbf{E} = (\nabla\mathbf{u} + \nabla\mathbf{u}^T)/2$ and $\hat{\mathbf{e}}_\alpha$ ($\alpha = 1, 2, 3$) are the corresponding eigenvectors. In an purely extensional flow, the polymers are aligned with the extensional direction, i.e. $r_1^2 \simeq 1$ and $r_3^2 \simeq 0$, and stretched by the extensional velocity gradient, thus

$$\frac{1}{Wi} \frac{\|\mathbf{h}\|^2}{1 - \|\mathbf{h}\|^2} \simeq E_{11}. \quad (3.3)$$

In a pipe flow, the topology can be different and the polymers are not generally aligned with the extensional direction, thus the difference $r_1^{(j)2} - r_3^{(j)2}$ is less than 1. Nonetheless, the effect is caused by large polymer extension, thus the extensional viscosity provided by N_{ext} extended polymers (the ones with $H > H_{ext} \approx 1$) can be estimated as

$$\Delta\eta \simeq \frac{\beta}{2} \sum_{j=1}^{N_{ext}} \frac{\delta(\mathbf{x} - \mathbf{x}_c^{(j)})}{c_o}. \quad (3.4)$$

Averaging over the domain, it follows that

$$\Delta\eta \propto \beta \frac{c_{ext}}{c_o} = \beta \frac{c_{H>H_{ext}}}{c_o}, \quad (3.5)$$

where the quantity $c_{H>H_{ext}}/c_o$ is the fraction of the polymers extended beyond H_{ext} . This quantity is a function of Wi_τ and is computed from a set of simulations with monodisperse solutions with $\beta = 60$ at $Re_\tau = 180$, fixing $H_{ext} = 0.8$. It is shown in figure 4 using blue dots, alongside the drag reduction measured (red dots). The two curves display a similar trend: both the number of extended polymers and drag reduction starts increasing

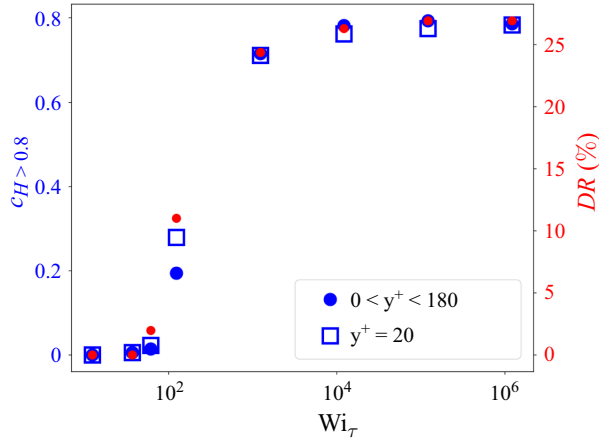


Figure 4. Fraction of polymers extended beyond $H_e = 0.8$ (blue symbols) and drag reduction (DR, red symbols) versus the Weissenberg number Wi_τ .

above a threshold (approximately $Wi_\tau = 50$) and are asymptotic with the Weissenberg number. The existence of a threshold explains why, in the polydisperse solution, the low molecular weight polymers have zero effect, despite the polymer concentration, and thus the polymer viscosity β , being significantly higher compared with the few high molecular weight polymers, see figure 1(b). Considering the linear dependence between drag reduction after onset and β , the analysis leads to the conclusion that there exists a proportionality between the amount of drag reduction and the increased viscosity

$$DR \propto \Delta\eta \propto \beta \frac{c_{ext}}{c_o}. \quad (3.6)$$

A small discrepancy between the number of extended polymers and drag reduction appears at Weissenberg numbers very close to the onset, at which the number of extended polymers is not very large. The difference can be significantly reduced if the extended polymers' statistics are restricted to the buffer zone, where turbulent velocity gradients are higher and polymers are most likely to be stretched. The difference between local and global averages reduces as the Weissenberg number increases since smaller velocity gradients are needed to stretch the polymers.

To conclude, we remark that the relation (3.6) is expected to be valid for moderate drag reduction, as the linear dependence on β cannot in fact explain the saturation at maximum drag reduction.

4. Conclusions

By DNSs of a polydisperse polymer solution, we showed that drag reduction is obtained when the turbulent velocity field fully extends a sufficient number of polymers. Simulation results show excellent quantitative agreement with the experiment of Berman (1977). In a monodisperse DNA solution, the polymers are easily extended to full length and, being unable to elongate more, strongly alter the turbulent flow by locally modifying the viscosity field (Serafini *et al.* 2022). In a polydisperse solution, the role of fully elongated polymers remains crucial. When the longest polymers of the distribution have a Weissenberg number that is large enough to allow for a sufficient number of fully stretched polymers, the onset of drag reduction occurs.

The conclusion is that full elongation is the essential ingredient to explain the onset of drag reduction, even in the case of polydisperse solutions for which a characterisation in terms of bulk parameters (concentration and Weissenberg number) is meaningless.

An interpretation of our results is possible in terms of a time criterion, similar to the one proposed by Lumley (1969). In particular, we observe drag reduction when the Weissenberg number is large enough such that fully stretched polymers appear in the suspension. This scenario is realised when the Weissenberg number of the highest molecular weight polymers is approximately $Wi_{\tau} = 50$ and their concentration is order 1 wppm. In most of the experiments, concentrations hundreds of times larger are needed to compensate for the small occurrence of fully stretched polymers.

Acknowledgements. Computational resources were provided by CINECA under the Leonardo Early Access Program (LEAP), IscraB #HP10BBQ4BV and EuroHPC grant EUHPC-R 02-167.

Funding statement. This work has received financial support from Sapienza (Project RG12117A66DC803E) and ICSC – Centro Nazionale di Ricerca in ‘High-Performance Computing, Big Data and Quantum Computing’, funded by European Union – NextGenerationEU.

Declaration of interests. The authors report no conflict of interest.

REFERENCES

- ALVES, M.A., OLIVEIRA, P.J. & PINHO, F.T. 2021 Numerical methods for viscoelastic fluid flows. *Annu. Rev. Fluid Mech.* **53** (1), 509–541.
- BATTISTA, F., MOLLICONE, J.-P., GUALTIERI, P., MESSINA, R. & CASCIOLA, C.M. 2019 Exact regularised point particle (erpp) method for particle-laden wall-bounded flows in the two-way coupling regime. *J. Fluid Mech.* **878**, 420–444.
- BENZI, R., D.E. ANGELIS, E., L VOV, V.S., PROCACCIA, I. & TIBERKEVICH, V. 2006 Maximum drag reduction asymptotes and the cross-over to the newtonian plug. *J. Fluid Mech.* **551** (-1), 185–195.
- BERMAN, N.S. 1977 Drag reduction of the highest molecular weight fractions of polyethylene oxide. *Phys. Fluids* **20** (5), 715–718.
- BIRD, R.B., CURTISS, C.F., ARMSTRONG, R.C. & HASSAGER, O. 1987 In *Dynamics of Polymeric Liquids*, vol. 2, Kinetic Theory. Wiley.
- BRANDFELLNER, L., MURATSPAHIĆ, E., BISMARCK, A. & MÜLLER, H.W. 2024 Quantitative description of polymer drag reduction: effect of polyacrylamide molecular weight distributions. *J. Non-Newton. Fluid Mech.* **325**, 105185.
- CHOI, H.J., LIM, S.T., LAI, P.-Y. & CHAN, C.K. 2002 Turbulent drag reduction and degradation of dna. *Phys. Rev. Lett.* **89** (8), 088302.
- DE ANGELIS, E., CASCIOLA, C.M. & PIVA, R. 2002 Dns of wall turbulence: dilute polymers and self-sustaining mechanisms. *Comput. Fluids* **31** (4-7), 495–507.
- DE GENNES, P.G. 1986 Towards a scaling theory of drag reduction. *Physica A: Statis. Mech. Appl.* **140** (1-2), 9–25.
- DIMITROPOULOS, C.D., SURESHKUMAR, R. & BERIS, A.N. 1998 Direct numerical simulation of viscoelastic turbulent channel flow exhibiting drag reduction: effect of the variation of rheological parameters. *J. Non-Newton. Fluid Mech.* **79** (2-3), 433–468.
- DOI, M., EDWARDS, S.F. & EDWARDS, S.F. 1988 *The Theory of Polymer Dynamics*. Vol. 73. oxford University Press.
- DU, Y. & KARNIADAKIS, G.E. 2000 Suppressing wall turbulence by means of a transverse traveling wave. *Science* **288** (5469), 1230–1234.
- ESCUDIER, M.P., PRESTI, F. & SMITH, S. 1999 Drag reduction in the turbulent pipe flow of polymers. *J. Non-Newton. Fluid Mech.* **81** (3), 197–213.
- GUALTIERI, P., PICANO, F., SARDINA, G. & CASCIOLA, C.M. 2015 Exact regularized point particle method for multiphase flows in the two-way coupling regime. *J. Fluid Mech.* **773**, 520–561.
- LUMLEY, J.L. 1969 Drag reduction by additives. *Annu. Rev. Fluid Mech.* **1** (1), 367–384.
- LUMLEY, J.L. 1973 Drag reduction in turbulent flow by polymer additives. *J. Polym. Sci. Macromol. Rev.* **7** (1), 263–290.
- MAXEY, M.R. & RILEY, J.J. 1983 Equation of motion for a small rigid sphere in a nonuniform flow. *Phys. Fluids* **26** (4), 883–889.

- MCCOMB, W.D. & RABIE, L.H. 1982 Local drag reduction due to injection of polymer solutions into turbulent flow in a pipe. part ii: laser-doppler measurements of turbulent structure. *AIChE J.* **28** (4), 558–565.
- MIN, T., YOO, J.Y., CHOI, H. & JOSEPH, D.D. 2003 Drag reduction by polymer additives in a turbulent channel flow. *J. Fluid Mech.* **486**, 213–238.
- PROCACCIA, I., L'VOV, V.S. & BENZI, R. 2008 Colloquium: theory of drag reduction by polymers in wall-bounded turbulence. *Rev. Mod. Phys.* **80** (1), 225–247.
- SERAFINI, F., BATTISTA, F., GUALTIERI, P. & CASCIOLA, C.M. 2022 Drag reduction in turbulent wall-bounded flows of realistic polymer solutions. *Phys. Rev. Lett.* **129** (10), 104502.
- SERAFINI, F., BATTISTA, F., GUALTIERI, P. & CASCIOLA, C.M. 2023 The role of polymer parameters and configurations in drag-reduced turbulent wall-bounded flows: comparison between fene and fene-p. *Intl J. Multiphase Flow* **165**, 104471.
- SERAFINI, F., BATTISTA, F., GUALTIERI, P. & CASCIOLA, C.M. 2024 Polymers in turbulence: any better than dumbbells? *J. Fluid Mech.* **987**, R1.
- SREENIVASAN, K.R. & WHITE, C.M. 2000 The onset of drag reduction by dilute polymer additives, and the maximum drag reduction asymptote. *J. Fluid Mech.* **409**, 149–164.
- SURESHKUMAR, R., BERIS, A.N. & HANDLER, R.A. 1997 Direct numerical simulation of the turbulent channel flow of a polymer solution. *Phys. Fluids* **9** (3), 743–755.
- TABOR, M. & DE GENNES, P.G. 1986 A cascade theory of drag reduction. *EPL (Europhys. Lett.)* **2** (7), 519–522.
- TOMS, B.A. 1949 *Proceedings of the 1st International Congress On Rheology*, pp. 135. Vol. II. North Holland.
- TURISINI, M., AMATI, G. & CESTARI, M. 2024 Leonardo: a pan-European pre-exascale supercomputer for HPC and AI applications. *JLSRF* **8**, A186.
- VINCENZI, D., PERLEKAR, P., BIFERALE, L. & TOSCHI, F. 2015 Impact of the peterlin approximation on polymer dynamics in turbulent flows. *Phys. Rev. E* **92** (5), 053004.
- VIRK, P.S. 1975 Drag reduction fundamentals. *AIChE J.* **21** (4), 625–656.
- XI, L. 2019 Turbulent drag reduction by polymer additives: fundamentals and recent advances. *Phys. Fluids* **31** (12), 121302.
- ZHOU, Q. & AKHAVAN, R. 2003 A comparison of fene and fene-p dumbbell and chain models in turbulent flow. *J. Non-Newton. Fluid* **109** (2-3), 115–155.